Numerical Methods in Civil Engineering, 9-4 (2025) 9-23

Numerical Methods in Civil Engineering

Journal Homepage: https://nmce.kntu.ac.ir/

Seismic Evaluation of Composite Steel Moment Frames with Brace Members and Rotational Friction Dampers under Near-Fault Earthquakes

Ali Sattari *, Ahmad Maleki **, Mohammad Ali Lotfollahi-Yaghin***

ARTICLE INFO

RESEARCH PAPER

Article history:
Received:
February 2022
Revised:
January 2025
Accepted:
February 2025

Keywords:
Composite steel moment frame,
Base shear,
Energy dissipation,
Rotational friction damper,
Hysteresis curve.

Abstract:

Dampers are employed to improve the cyclic behavior of structures against wind- and earthquake-induced loads. Rotational friction dampers (RFDs) dissipate energy through reciprocal rotation. The present research investigates the behavior of steel frames with concrete-filled columns under three different frames of identical configurations for beams and columns but different positions for the bracing and RFD systems to see the effect of eliminating a part of the bracing member. Two loading schemes were considered to study the behavior of the introduced frames. In the first stage, the frames were subjected to vertical loading coupled with a cyclic load at the beam level. In the second stage, however, the cyclic load at beam level was replaced with earthquake acceleration at the structure base. All sample frames were then modeled and analyzed in finite-element software. Applying the bracing system coupled with the RFD reduced the base shear compared to the structure without the bracing and RFD systems, although the reduction was not the same for all frames with different bracing schemes. Moreover, compared to the frame without the RFD, the damper could limit the structural drift in 6 models, though it boosted the drift in 1 model. Results showed that RFDs can dissipate seismic energy through rotational friction slippage. The dampers could dissipate up to 90% of the energy induced by lateral loads to the structure. Also, removing a portion of the bracing member was found to be useful for architectural purposes.

1. Introduction

Various - energy dissipation systems have been investigated to protect structures and their inhabitants against wind and earthquake forces. The braced frame is the most common form of frame resistance against lateral forces in steel structures. The concentrically braced frames, although economical and highly stiff, have several shortcomings such as buckling of the bracing member. In addition, they also have architectural limitations concerning the execution of openings, which could be improved by using the new devices for energy dissipation and their proper combination with the structure. The idea of using CFT (concrete-filled tube) steel frames with bracings and rotational friction dampers is presented to enhance the performance of steel frames. The present research has introduced a seismic retrofitting plan, in which several rotational friction dampers are connected to the beams and columns at the corners of the steel frame. In the previous research, the rotational friction dampers were mainly parts of the bracing system placed at the beginning, end, or middle of the bracing member. In the present scheme, the diagonal member of the bracing has been ultimately removed. Another advantage of this scheme is that during severe earthquakes the bracing would not suddenly experience nonlinear deformations and the lateral strength of the structure would not diminish at the next cycles or stronger earthquakes under diminished strength and stiffness. On the other hand, rotational friction dampers could lead to further energy dissipation in systems that lack dampers. Among the main characteristics of near-field

**Ph.D student of Earthquake Engineering, Department of Civil Engineering, Islamic Azad University, Maragheh Branch, Maragheh, Iran.*
***Corresponding author: Assistant Professor, Department of Civil Engineering, Islamic Azad University Maragheh Branch, Maragheh, Iran. Email: ad.maleki@iau.ac.ir*
**** Professor, Department of Civil Engineering, University of Tabriz, Tabriz, Iran.*

https://doi.org/10.61186/NMCE.695.1

earthquakes are the lack of wide bands of corresponding accelerograms and the presence of pulse-like characteristics. One of the most critical characteristics of earthquakes in the near field is that such earthquakes are not broadband and have pulse-type properties. One of the most critical characteristics of near-field earthquakes is the superiority of the wave-like over the mode-like behavior of the structure. Ambraseys et al. [1-2] [3] investigated the near-field horizontal and vertical earthquake ground motions. Considering the difference between near-fault and far-fault ground motions, Somerville[4], investigated the engineering characterization of near-fault ground motions. Kohrangi et al. [5] investigated the pulse-like versus non-pulse-like ground motion records. Khansefid [6] studied the pulse-like ground motions of the Iranian plateau. Xu et al. [7] inspected a combined rotational damper. Sajad Veismoradi et al. [8] analytically examined a new self-centering rotational friction damper. Javidan et al. [9] developed a seismic resistance system containing a steel frame connected to the pin and rotational friction dampers. Mirzabagheri et al. [10] evaluated the performance of rotational friction dampers in several units of steel frames under lateral excitations and concluded that increasing the number of damper sheets would enhance energy dissipation. Through the analysis of 3-, 7-, and 12-story frames, they observed an improvement in the seismic behavior of the structure with rotational friction dampers. Eldin et al. [11] studied the slotted steel dampers with friction pads under cyclic loading. The test results showed that the dampers had stable behavior during the loading and a desirable performance in minimizing damage probability. Later, they investigated a 4-story structure, and the results agreed with the experimental findings. Kim et al. [12] investigated a new type of connection, including post-tensioned elements, to present a self-centering capacity and friction mechanism for energy dissipation, concluding that the frictional behavior of the friction damper was stable, repeatable, and predictable. Kim et al. [13] investigated three 12-story structures with slotted dampers. They performed the optimal distribution of steel and dampers and concluded that the seismic responses of the base shear were reduced, with a difference of <10% in the three models. Kim et al. [14] studied the optimal distribution of friction dampers for a concrete structure and concluded that friction dampers reduced the inter-story drift by 30-40% and dissipated about 70% of the lateral force. Anooshehei et al. [15] [16]experimentally examined the cyclic behavior of friction dampers having metal pads with alloys of aluminum, ST37 steel, and galvanized steel. According to the acceptance criteria, they concluded that the abrasion of ST37 steel and galvanized steel was high, but the aluminum pad was acceptable and could be replaced after the earthquake. Jarrahi et al. [17] investigated the simultaneous optimization of the location and friction parameters of the rotational friction damper. The optimization results revealed that a portion of the input energy was absorbed by the rotational friction damper, simultaneously reducing its value. Increasing the rotational friction dampers at the optimal locations could guarantee the structure under a real earthquake. Morgen et al. [18] evaluated the seismic response of pre-fabricated concrete frames with friction dampers and concluded that the friction damper caused further energy dissipation in the frame. Moradi et al. [19] investigated the new ideas in terms of controlling vibration in structures using friction dampers and concluded that the presence of friction dampers could reduce the seismic demand in the structural members. The behavior of friction dampers depended on the sliding surface and could further dissipate energy at small displacements, raising their potential application in concrete structures. Bonchev et al. [20] studied the rotational friction dampers as links between columns and examined several steel frames with different stories, concluding that the rotational friction damper reduced the base shear and structure displacement values, with no need for maintenance throughout the structure's life. Montuori et al. [21] presented a new method, known as the plastic mechanism theory, for designing an earthquake-resistant system by combining a moment-resisting frame and a bracing system equipped with friction dampers. They concluded that friction dampers caused a reduction in the inter-story drift, thus reducing damage to the structure. Naeem et al. [22-23] studied the seismic retrofitting of structures using rotational friction dampers with restoring force. The damper consisted of a rotational friction pad with strong helical springs. Residual deformation in the structure of dampers was one of the problems concerning the use of passive dampers for protection against earthquakes, reducing the operational efficiency. Nevertheless, this structure could return to its original state. Qu et al. [24-25] performed an experimental study on the friction damper equipped with brake pads between steel sheets in the space between two shear walls. The designed dampers in the connecting beams could greatly enhance the seismic performance of the structure. The friction pads in both conducted tests revealed a stable hysteresis response with complete energy dissipation. Barzegar et al. [26] numerically evaluated the friction damper, investigating a 5-story structure under seismic loading and a 20-story structure under seismic and wind loads separately. The results showed that dampers with maximum capacity did not have an optimal performance. Shirkhani et al. [27] performed time history analyses on 3-, 7-, and 12-story steel frames to investigate their behavior, concluding that the friction damper reduced the stories' drift and their maximum displacement. Shariatmadar et al. [28] presented a practical and efficient method for precise modeling and proposed a simple model of buckling–restrained bracings. Yildirim et

al. [29] performed a case study that included seismic retrofitting of an industrial structure made of steel frame with prefabricated concrete peripheral walls. They concluded that friction dampers helped maintain the desired performance goals. Langley et al. [30] performed some experiments on the rotational friction dampers in an industrial frame with concrete walls, indicating that the rotational friction damper could significantly dissipate energy. The results proved that the connection could bear large displacements without losing strength and sustaining the design load. Zahrai et al. [31] studied a structure with bracings and friction dampers and concluded that friction dampers could reduce the dynamic load functioning on the structure. Hosseini et al. [32] examined the seismic performance of a novel structural system with cyclic motions and columns equipped with friction dampers at the base level. They concluded that the novel structural system led to the more economic design of columns in ordinary buildings. Guo et al. [33] studied the performance of friction dampers for the seismic response control in a high-speed railway bridge-track system. They concluded that the rotational friction damper contributed effectively to improving the seismic performance of the bridge structure. Zhang et al. [34] studied the self-centering steel frames with intermediate columns containing friction dampers and concluded that the friction damper could increase the global lateral stiffness while also protecting the main components of the system. Oance et al. [35] investigated the seismic analysis of steel structures using friction dampers and concluded that considering the relative independence of the dampers under environmental conditions, the friction dampers were appropriate options for the structural capacity improvements in terms of energy dissipation. Santos et al. [36] evaluated the friction dampers' response against impact loads with large strains, concluding that the impact loads with large strains increased the friction damper force and reduced the ductility capacity. These friction dampers create a type of sliding joint. Beheshti-aval et al. [37] investigated a hybrid friction damper with a concentrically braced steel frame and concluded that energy was dissipated by friction in weak to intermediate ground motions, but energy was absorbed by yielding in strong ground motions. In addition, they could be utilized to retrofit existing buildings with narrow bracing members designed solely based on tension. These dampers could easily be substituted with new dampers in case of damage after a strong earthquake. Zhang et al. [38] proposed a prestressed steel frame with intermediate columns containing friction dampers for a large span in an active seismic zone and an important valuable structure. Tafakori et al. [39] investigated the application of friction dampers in tall steel buildings and concluded that increasing damping in a structure could adversely affect the structure's performance in some cases. Taiyari et al. [40] inspected a damage-based design method for a multi-story structure with chevron-braced steel frames equipped with friction dampers, evaluating three multi-story steel frames based on the proposed method. They identified and analyzed the sliding force of the friction damper and the stiffness ratio of the system as two important factors and concluded that the highest damage corresponded to the sliding force higher or lower than the sliding force of the damper. Lee et al. [41] proposed a seismic design method for friction dampers based on the distribution of the shear force in the story and concluded that the sliding force of the damper was <0.3 of the shear force. Sanghai et al. [42] studied the optimal positioning of friction dampers in a building concerning soil nonlinearity and concluded that the friction dampers effectively limited plastic hinges in the main structure members. Furthermore, where the nonlinearity of soil was taken into consideration, a lower number of friction dampers would be needed. Miguel et al. [43] presented a new method in the frequency domain for the simultaneous optimal design of positions and the number of friction dampers. Saeed-monir et al. [44] investigated a modified friction damper for diagonal bracing of structures and concluded that the proposed damper showed a stable hysteresis cycle under harmonic loading in the laboratory. It absorbed considerable force and reduced displacement and shear base values in the examined structure. Latour et al. [45] explored the beam-to-column connection equipped with a friction damper, investigating the beam-to-column connection with a friction damper in two states and highlighting improved connection performance by the friction damper. Suk et al. [46] studied the friction behavior of spherical (multi-directional) dampers and concluded that the shear load capacity of the damper did not change at different frequencies. Solaimani-nezhad et al. [47] studied the steel off-center bracing (y-shaped) with low ductility, equipped with a rotational friction damper, reporting reduced stiffness by 20-35% and increased energy dissipation by approximately 50%. Maleki et al. [48] investigated the behavior of steel frames with concrete-filled tubes in two states, including a structure with and without bracing and rotational friction dampers.

2. Structure modelling and configuration of the proposed models

The present article has modeled a new combination of composite steel frames (Figure 1), using CFT columns to increase the strength and bearing of the columns. The specimens included a frame with concrete-filled tube columns and IPE section beam and fixed connections, without bracings and rotational friction dampers (Figure 1-a), named the base frame. The second specimen, named the CFT-BM frame, was the base model incorporating horizontal and diagonal bracings with box sections, fixed

connections, and two series of rotational friction dampers (Figure1-b), named CFT-BM frame. Finally, the third specimen was a frame without diagonal bracing but with vertical bracing (Figuer 1-c), named CFT-M. It is worth noting that the dimensions and properties of the similar members were identical in all the specimens. the frame without bracing was made by ABAQUS software to investigate the performance of braced frame with rotational friction damper. The study considered composite columns with square box section of 30x30cm dimensions and 2.5cm thickness, IPE300 steel beam section and bracing with the box section of 12x12cm dimensions and 0.5cm thickness, CFT columns with beam and bracing, modeling other components of the frame as solid. The rotational friction dampers were made of steel plate (long plate with a 458-cm length, 15-cm width, and 1-cm thickness and short plate with a 33-cm length, 15-cm width, and 1-cm thickness). The Tie constraint was implemented to model the welded edges to the structure, and surface-to-surface Contact constraint was used in the software to define sheets with contact.

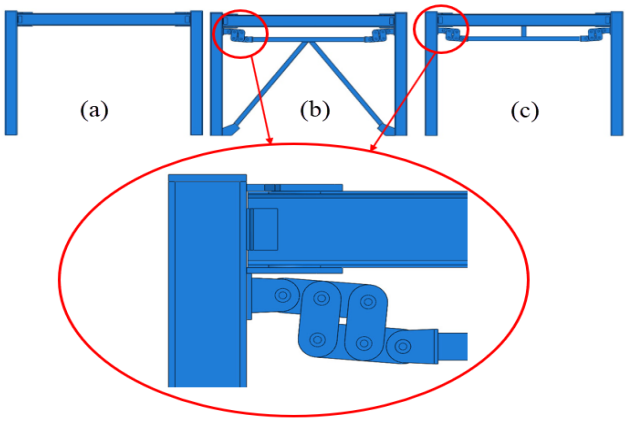

Fig. 1: a) CFT frame b) CFT-BM frame c) CFT-M frame

The rotational friction damper is shown in Figure 2.

Fig. 2: Rotational friction damper

3. Validation

First, the laboratory specimen in research conducted by Mualla et al. [49] (numerically shown in Figure 3) was modeled using the finite element software ABAQUS. Then, the specimen was subjected to lateral load (shown as displacement in Figure 4). The axial load generated due to the displacement was then derived from the results of numerical analysis to draw the corresponding hysteresis curve. The finite element analysis results agreed with the results obtained from the laboratory specimen (Figure 5-a). - Subsequently this model - was analyzed under the influence of the Elcentro-NS acceleration component. The - analysis outcome were in good agreement with the results presented for the laboratory sample. It is shown in (Figure 5-b).

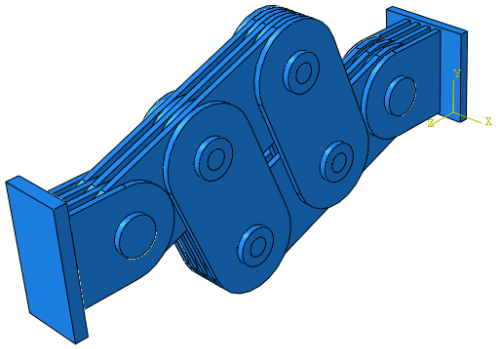

Fig. 3: Specimen of the rotational friction damper modeled for validation

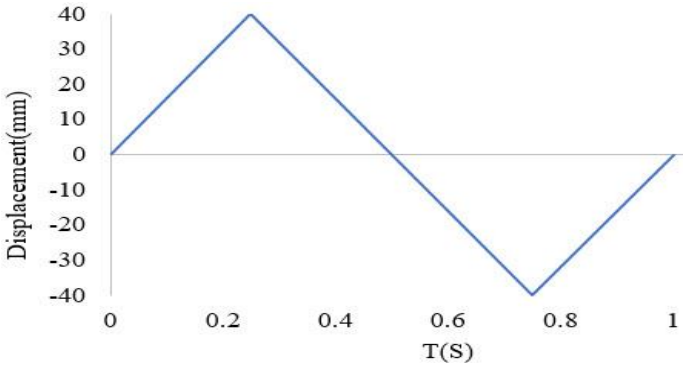

Fig. 4: Diagram of applied displacement on the modeled laboratory specimen

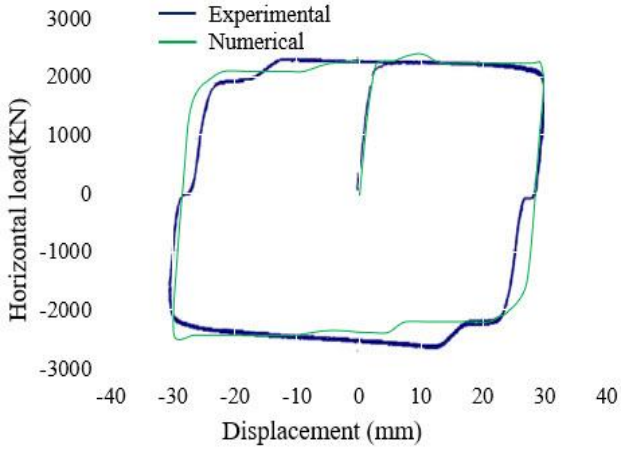

(a)

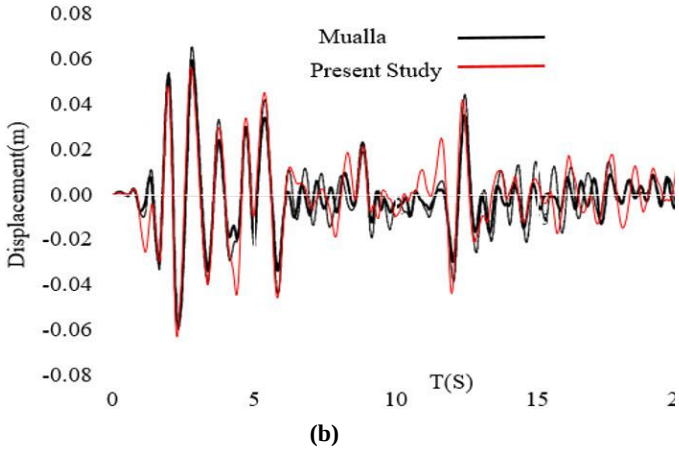

Fig. 5: a) Comparison between the hysteresis curves of the laboratory specimen by Mualla et al. [49] and the finite element analysis results, b) Comparison of the location change diagram of Movala et al.'s laboratory sample with limited implementation analysis

4. Analytic relationships

Figure 6 presents the rotational friction damper and the position of the parameters used in the relationships. Also, Figure 7 illustrates the schematic diagram for theoretical calculations.

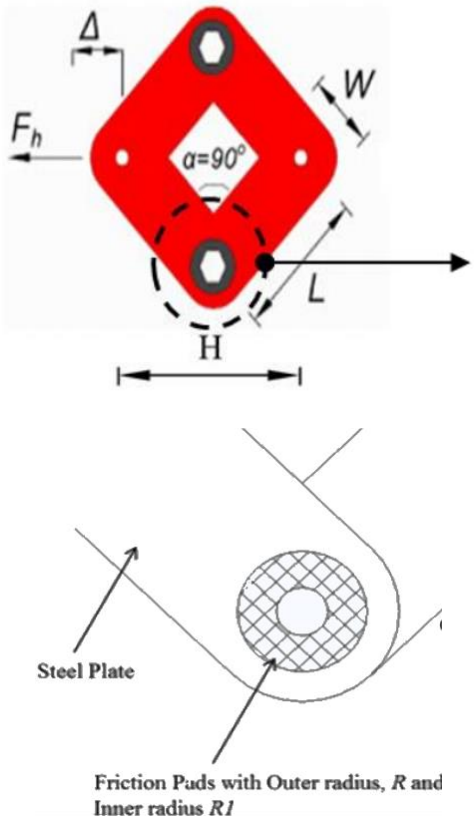

Fig. 6: Rotational friction damper [48]

The research results of Guo et al. [33], Shrestha et al. [50], Chen et al [51], and those obtained by Kim et al.[52] were utilized to calculate the stiffness of the rotational friction damper.

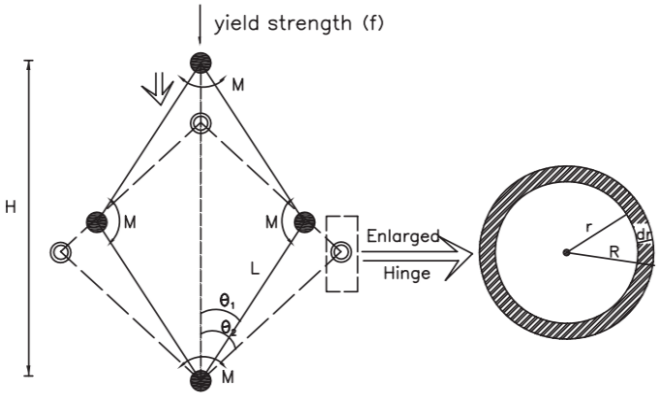

Fig. 7: Simplified schematic diagram for theoretical calculations [51]

The applied load on the rotational friction damper is calculated from Equation (2):

$$M = \int_{R1}^{R} dM = \int_{R1}^{R} 2\pi r^2 \mu p dr = \frac{2}{3}\pi\mu p(R^3 - R_1^2) \quad (1)$$

$$F_h = \frac{nM}{\sqrt{L^2 + (H/2)^2}} = \frac{nM}{L\cos(\alpha/2)} \quad (2)$$

$$H_1 = 2L\cos\theta_1 \quad (3)$$

$$\theta_2 = \theta_1 + d\theta \quad (4)$$

$$H = H_1 - H_2 = 2L(\cos\theta_1 - \cos(\theta_1 + d\theta)) \quad (5)$$

In the above equations, F_h is the rotational friction force at each joint, M represents the resistant moment against rotational friction at each hinge, n shows the number of hinges, L is the effective length of the sheet, with the location of α angle shown in Figure 6. Also, μ represents the friction coefficient, P is the unit load, R_1 indicates the inner radius of friction pad, and R is the outer radius. Here, θ_1 and θ_2 are the included angles before and after deformation, and H_1 and H_2 indicate the respective heights before and after deformation. H is the height of the friction damper before and after rotation, calculated from Equation (5).

To perform structural analysis in the present study, the structures were subjected to cyclic loading based on the loading protocol for displacement generated under seven near-field ground motion records taken from the PEER website. The characteristics of these seven earthquakes are given in Table 1.

Table 1: Properties of the accelerograms

Earthquake	Station	Year	PGA (g)	Vs30 m/sec	Rjb (km)
Imperial valley	El Centro	1940	6.95	213.4	6.09
Northridge	Beverly Hills	1994	6.69	355.8	23.50
San Fernando	Hollywood Star	1971	6.91	316.4	22.77
Tabas	Boshrooyeh	1978	7.35	324.5	24.07
Duzce	Bolu	1999	7.14	293.5	12.02
Kobe	Amagasaki	1995	6.9	256	11.34
Kobe	Kakogawa	1995	6.9	213	22.50

Here, Vs. 30 Shear wave speeds up to a depth of thirty meters from the earth's surface. As shown in the table, Rjb is the distance of the site to the imaged surface from the rupture site, and fb0/fc0 represents the ratio of initial biaxial compressive yield stress to initial uniaxial compressive yield stress, with a default value of 1.12. Finally, Kc is the ratio of the second stress invariant on the tensile meridian to the compressive meridian at the initial yield, with the default value of 2/3 (Abaqus User Manual, 2008).

Tables 2 and 3 show the mechanical properties of concrete material and the strength properties of steel material, respectively.

Table 2: Mechanical properties of the concrete material [48]

Density (kg/m^3)	Poisson's Ratio	Compressive Strength (MPa)	Dilation Angle (deg.)	Fb_0/Fc_0	K	Eccentricity	Viscosity
2400	0.14	13-15	38	1.12	0.666	0.1	0.001

Table 3: Mechanical properties of the steel material

Density (kg/m^3)	Elasticity Modulus	Poisson's Ratio	Yield Stress (MPa)	Ultimate Strength (MPa)	Ultimate Strain (%)
7850	196	0.3	393	479	0.015

5. Loading in ABAQUS software

The beam was exposed to a load of 1.8 tons per meter length and adequate lateral support. The load on the left and right columns was 97.14 and 96.42 tons, respectively. The lateral loading applied on the columns was according to "Instructions for using dampers in design and strengthening of buildings" [53] and ASCE 7-16 [54-55] (Figure 8)

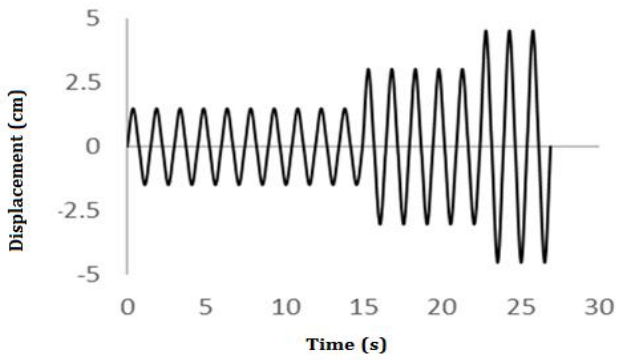

Fig. 8: Loading protocol applied to the specimens[48]

Figure 9 shows the position of the loads, the distance between the center of columns, and the height of the frame up to the position of applied cyclic load for the braced steel frame with composite columns and rotational friction dampers in the CFT-BM specimen (The dimensions and loading of all the specimens were identical).

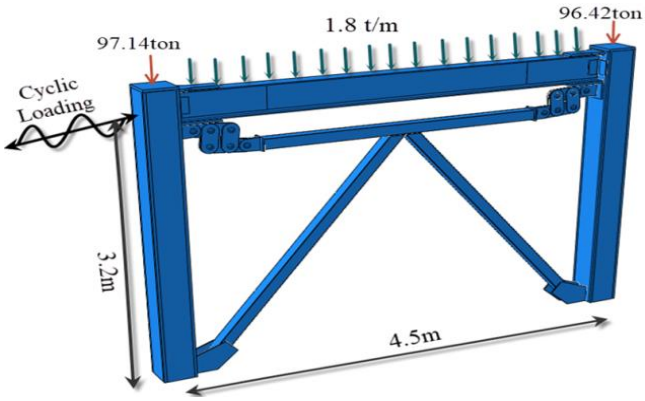

Fig. 9: Braced frame with rotational friction dampers in CFT-BM specimen[48]

6. Discussion and investigation of results

Figures 10-16 show the base shear values of frames (under cyclic loading according to the loading protocol for displacement generated by seven near-field ground motion records acting on the structure).

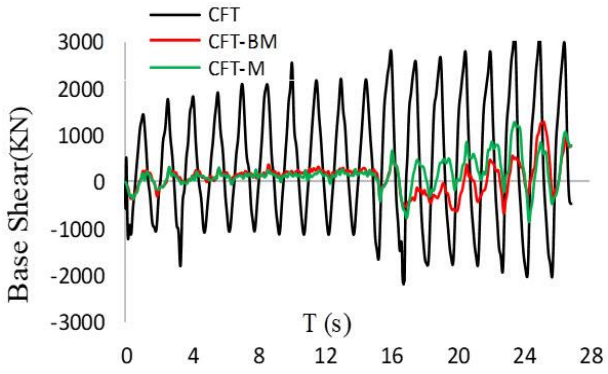

Fig. 10: Base shear diagram under the Northridge Earthquake

The results obtained from the loading of the specimens studied under Northridge loading show that the maximum base shear value was 3045 KN, 1103 KN, and 1138 KN in the base, CFT-BM, and CFT-M frames, respectively. In other words, the presence of the damper caused a 60% reduction in the base shear value in the CFT-BM frame and a 59% reduction in the base shear value in the CFT-M frame.

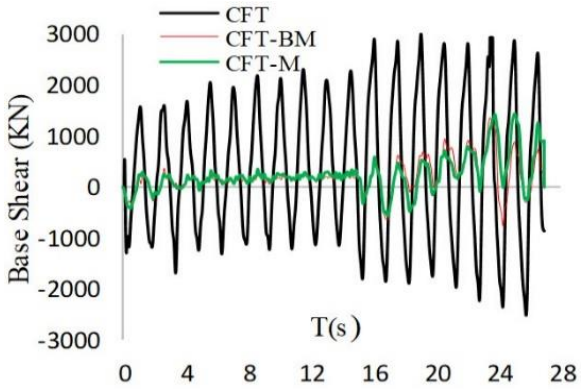

Fig. 11: Base shear diagram under Imperial Valley El Centro Earthquake

The results obtained from the loading of the specimens studied under Imperial Valley El Centro loading show that the maximum base shear value was 2943 KN, 1349 KN, and 1379 KN in the base, CFT-BM, and CFT-M frames, respectively. In other words, the presence of the damper caused a 54% reduction in the base shear value in the CFT-BM frame and a 53% reduction in the base shear value in the CFT-M frame.

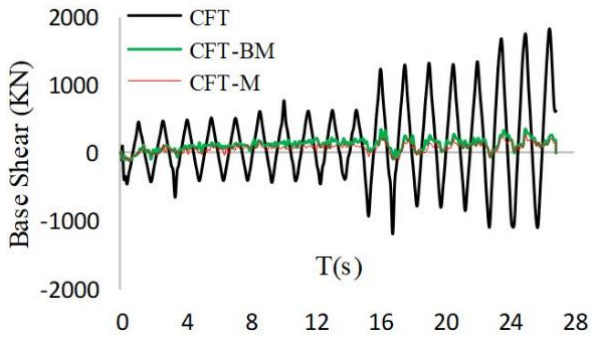

Fig. 12: Base shear diagram under Tabas Earthquake

The results obtained from the loading of the specimens studied under Tabas loading show that the maximum base shear value was 1800 KN, 221 KN, and 315 KN in the base, CFT-BM, and CFT-M frames, respectively. In other words, the presence of the damper caused an 87% reduction in the base shear value in the CFT-BM frame and an 82% reduction in the base shear value in the CFT-M frame.

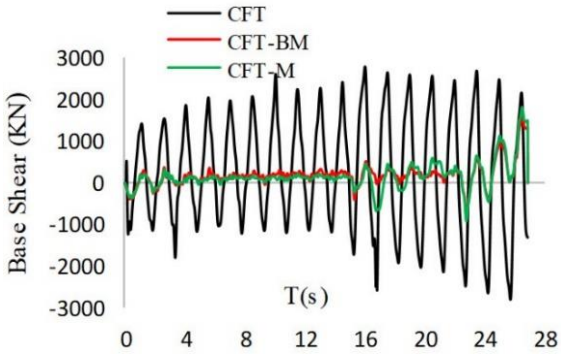

Fig. 13: Base shear diagram under Turkey Duzce Bolu Earthquake

The results obtained from the loading of the specimens studied under Turkey Duzce Bolu loading show that the maximum base shear value was 2713 KN, 1601 KN, and 1711 KN in the base, CFT-BM, and CFT-M frames, respectively. In other words, the presence of the damper caused a 41% reduction in the base shear value in the CFT-BM frame and a 37% reduction in the base shear value in the CFT-M frame.

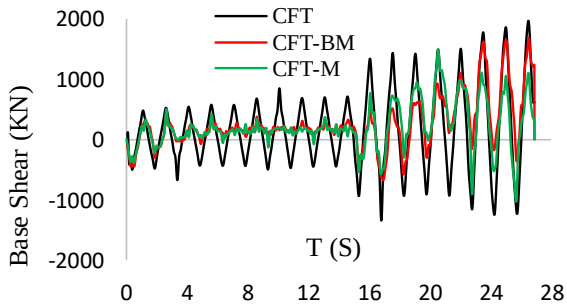

Fig. 14: Base shear diagram under KOBE Amagasaki Earthquake

The results obtained from the loading of the specimens studied under KOBE Amagasaki loading show that the maximum base shear value was 1966 KN, 1475 KN, and 1677 KN in the base, CFT-BM, and CFT-M frames, respectively. In other words, the presence of the damper caused a 25% reduction in the base shear value in the CFT-BM frame and a 15% reduction in the base shear value in the CFT-M frame.

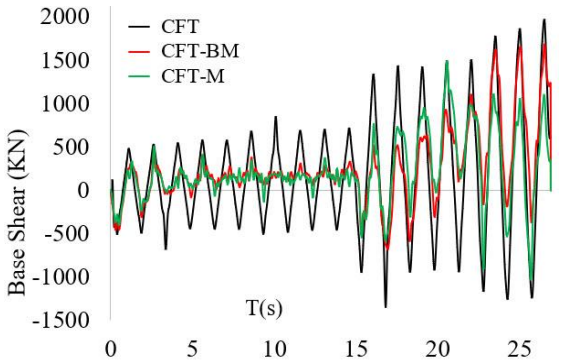

Fig. 15: Base shear diagram under the KOBE Kakogawa Earthquake

The results obtained from the loading of the specimens studied under KOBE Kakogawa loading show that the maximum base shear value was 1970 KN, 1314 KN, and 1555 KN in the base, CFT-BM, and CFT-M frames, respectively. In other words, the presence of the damper caused a 57% reduction in the base shear value in the CFT-BM frame and a 49% reduction in the base shear value in the CFT-M frame.

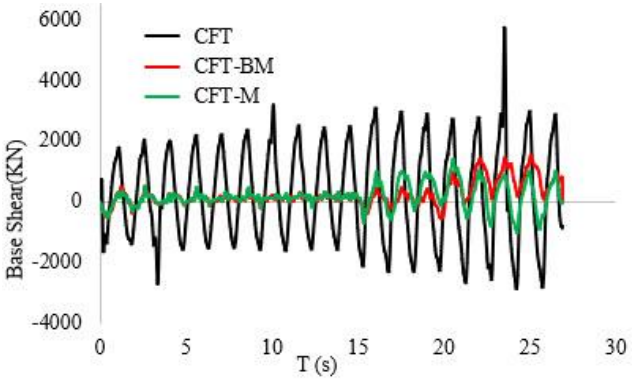

Fig. 16: Base shear diagram under San Fernando Earthquake

The results obtained from the loading of the specimens studied under San Fernando loading show that the maximum base shear value was 3727 KN, 1253 KN, and 1341 KN in the base, CFT-BM, and CFT-M frames, respectively. In other words, the presence of the damper caused a 66% reduction in the base shear value in the CFT-BM frame and a 64% reduction in the base shear value in the CFT-M frame.

7. Structure displacement due to applying earthquake acceleration to the structure base

The structures' displacements under earthquake acceleration for the introduced ground motions are shown in Fig**ure**s 17-23.

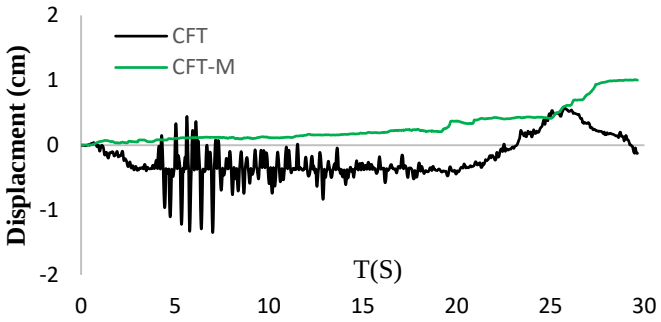

Fig. 17: Diagram of the structure displacement due to the Turkey Duzce Bolu earthquake acceleration

The results obtained from the loading of the studied specimens under Turkey Duzce Bolu loading indicate that the maximum displacement of the CFT frame was 1.4 cm at T=7 seconds and 1.00 cm at T=30 seconds in the CFT-M frame. Within the time interval of 0-20 seconds, the maximum displacement of the CFT-M frame was 0.3 cm, equal to 17% of the maximum displacement of the CFT frame within the same time interval.

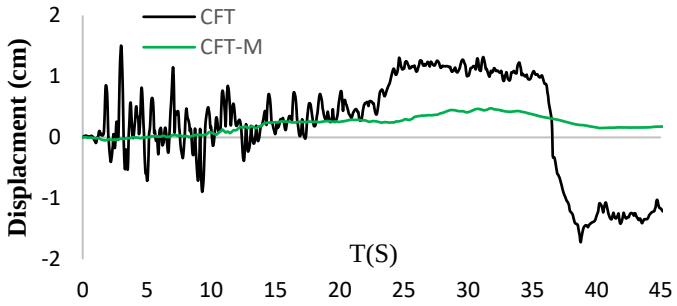

Fig. 18: Diagram of the structure displacement due to the San Fernando Hollywood Stor earthquake acceleration

The results obtained from the loading of the studied specimens under San Fernando Hollywood Stor loading indicate that the maximum displacement of the CFT frame was 1.8 cm at T=39 seconds and 0.50 cm at T=30 seconds in the CFT-M frame. Within the time interval of 0-45 seconds, the maximum displacement of the CFT-M frame was 0.5 cm, equal to 30% of the maximum displacement of the CFT frame within the same time interval.

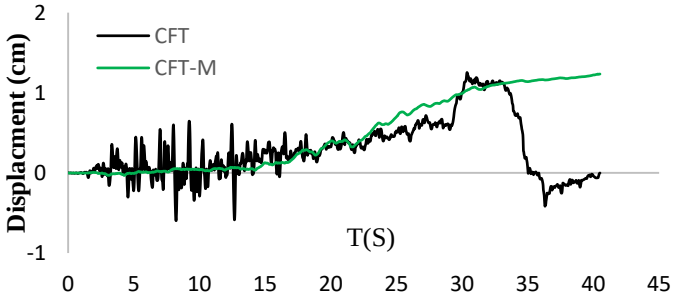

Fig. 19: Diagram of the structure displacement due to KOBE Kakogawa earthquake acceleration

The results obtained from the loading of the studied specimens under KOBE Kakogawa loading indicate that the maximum displacement of the CFT frame was equal to 1.3 cm at T=30 seconds and 1.3 cm at T=40 seconds in the CFT-M frame. Within the time interval of 0-20 seconds, the maximum displacement of the CFT-M frame was 0.3 cm, equal to 50% of the maximum displacement of the CFT frame within the same time interval.

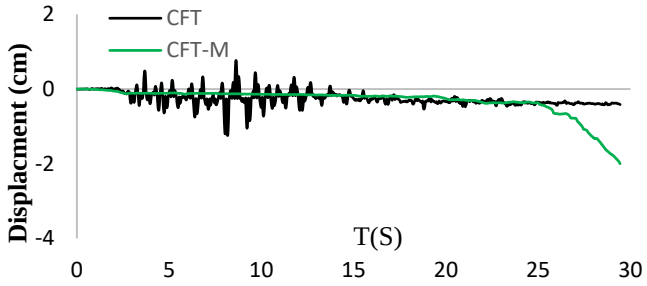

Fig. 20: Diagram of the structure displacement due to Northridge Beverly Hills earthquake acceleration

The results obtained from the loading of the studied specimens under Northridge Beverly Hills loading indicate that the maximum displacement of the CFT frame was 1.3 cm at T=8 seconds and 2.00 cm at T=30 seconds in the CFT-M frame. Within the time interval of 0-25 seconds, the maximum displacement of the CFT-M frame was 0.4 cm, equal to 31% of the maximum displacement of the CFT frame within the same time interval.

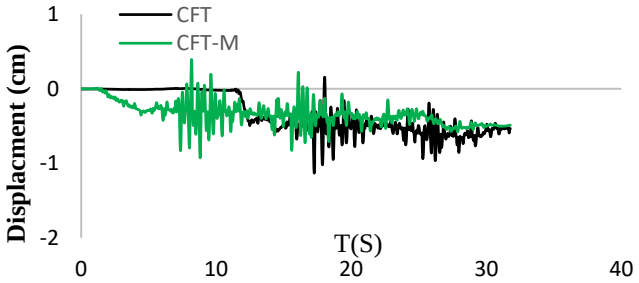

Fig. 21: Diagram of the structure displacement due to the KOBE Amagasaki earthquake acceleration

The results obtained from the loading of the studied specimens under KOBE Amagasaki loading indicate that the maximum displacement of the CFT frame was 1.2 cm at T=17 seconds and 0.9 cm at T=8 seconds in the CFT-M frame. Within the time interval of 0-30 seconds, the maximum displacement of the CFT-M frame was 0.9 cm, equal to 75% of the maximum displacement of the CFT frame within the same time interval.

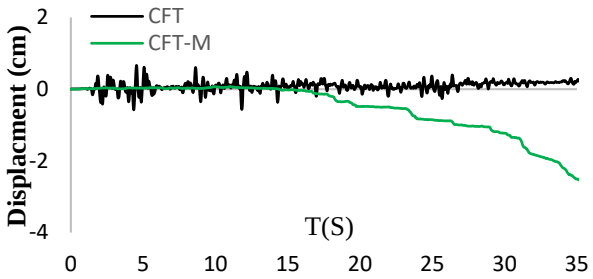

Fig. 22: Diagram of the structure displacement due to Imperial Valley El Centro earthquake acceleration

The results obtained from the loading of the studied specimens under Imperial Valley El Centro loading indicate that the maximum displacement of the CFT frame was 0.6 cm at T=12 seconds and 2.5 cm at T=35 seconds in the CFT-M frame. Within the time interval of 0-20 seconds, the maximum displacement of the CFT-M frame was 0.6 cm, equal to the maximum displacement of the CFT frame within the same time interval.

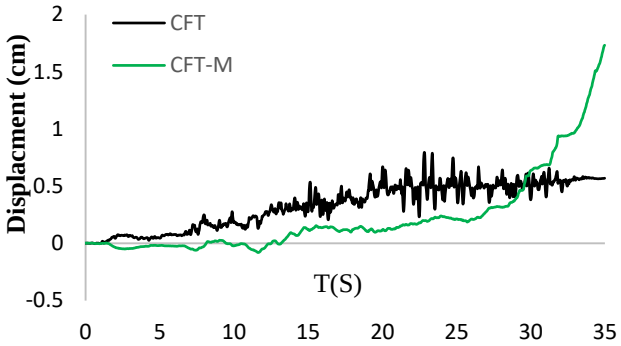

Fig. 23: Diagram of the structure displacement due to the Tabas Iran Boshrooyeh earthquake acceleration

The results obtained from the loading of the studied specimens under Iran Tabas Boshrooyeh loading indicate that the maximum displacement of the CFT frame was 0.8 cm at T=22 seconds and 1.7 cm at T=35 seconds in the CFT-M frame. Within the time interval of 0-30 seconds, the maximum displacement of the CFT-M frame was 0.3 cm, equal to 43% of the maximum displacement of the CFT frame within the same time interval.

8. Base shear of the structures due to applying earthquake acceleration to the structure base

Figures 24-30 show the base shear values of the structures under the earthquake acceleration for the introduced ground motion records.

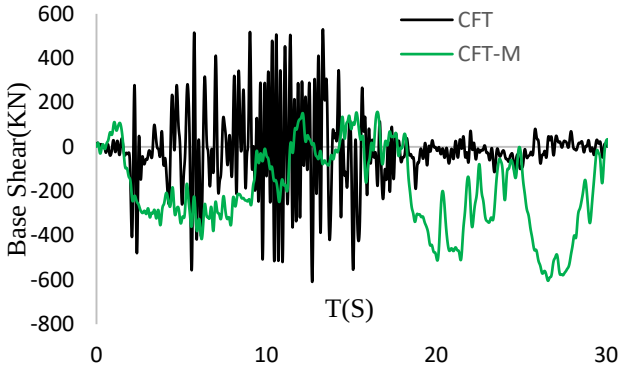

Fig. 24: Base shear of the structure under the Turkey Duzce Bolu earthquake acceleration

The results obtained from the loading of the studied specimens under Turkey Duzce Bolu loading indicate that the maximum base shear value of the CFT and CFT-M frames was 353 KN and 504 KN, respectively. In other words, the presence of the damper increased the base shear value by 43% in the CFT-M frame.

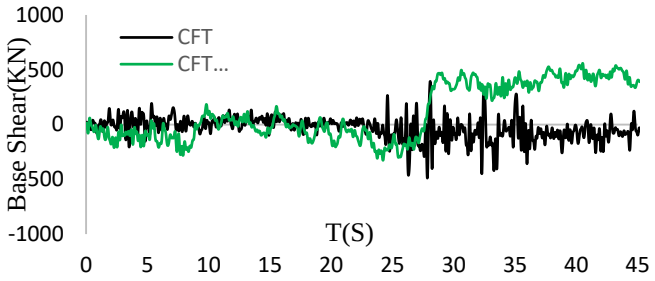

Fig. 25: Base shear of the structure under San Fernando Hollywood Stor earthquake acceleration

The results obtained from the loading of the studied specimens under San Fernando Hollywood Stor loading indicate that the maximum base shear value of the CFT and CFT-M frames was 490 KN and 548 KN, respectively. In other words, the presence of the damper increased the base shear value by 12% in the CFT-M frame.

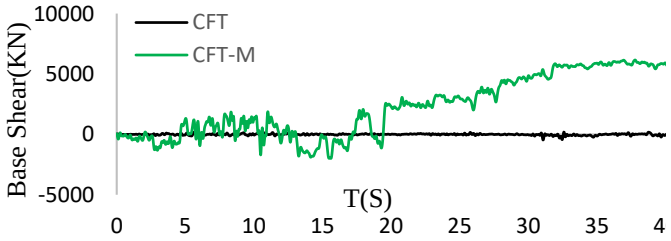

Fig. 26: Base shear of the structure under the KOBE Kakogawa earthquake acceleration

The results obtained from the loading of the studied specimens under KOBE Kakogawa loading indicate that the maximum base shear value of the CFT and CFT-M frames was 427 KN and 6117 KN, respectively. In other words, the presence of the damper increased the base shear value by 14 times that of the base shear in the CFT-M frame.

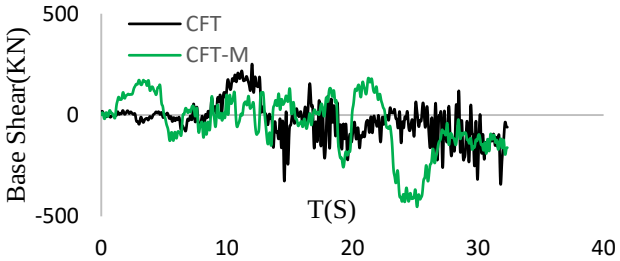

Fig. 27: Base shear of the structure under KOBE Amagasaki earthquake acceleration

The results obtained from the loading of the studied specimens under KOBE Amagasaki loading indicate that the maximum base shear value of the CFT and CFT-M frames was 342 KN and 451 KN, respectively. In other words, the presence of the damper increased the base shear value by 32% in the CFT-M frame.

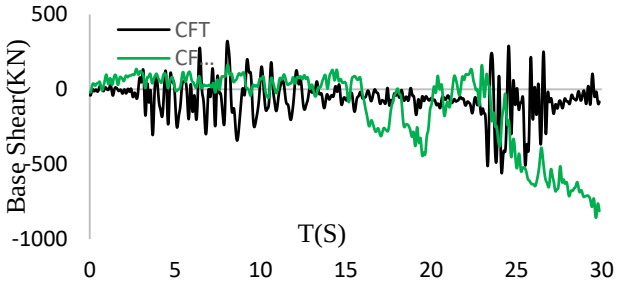

Fig. 28: Base shear of the structure under the Northridge, Beverly Hills earthquake acceleration

The results obtained from the loading of the studied specimens under the Northridge Beverly Hills loading indicate that the maximum base shear value of the CFT and CFT-M frames was 582 KN and 590 KN, respectively.

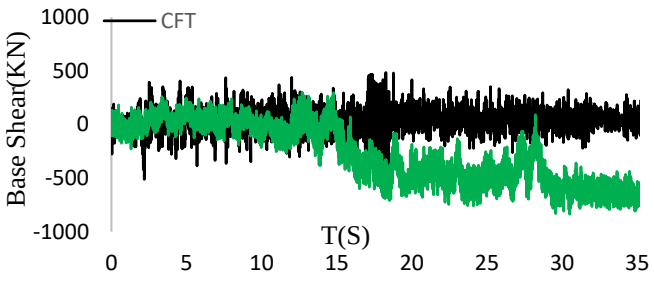

Fig. 29: Base shear of the structure under Imperial Valley El Centro earthquake acceleration

The results obtained from the loading of the studied specimens under Imperial Valley El Centro loading indicate that the maximum base shear value of the CFT and CFT-M frames was 513 KN and 838 KN, respectively. In other words, the presence of the damper increased the base shear value by 63% in the CFT-M frame.

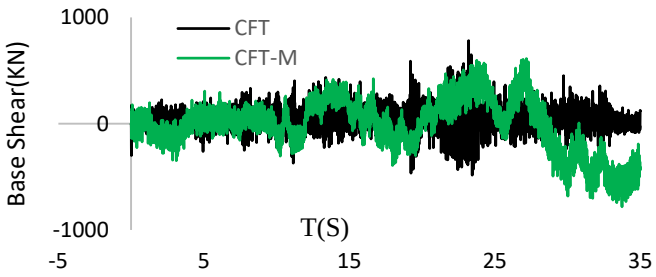

Fig. 30: Base shear of the structure under Iran Tabas Boshrooyeh earthquake acceleration

The results obtained from the loading of the studied specimens under Iran Tabas Boshrooyeh loading indicate that the maximum base shear value of the CFT and CFT-M frames was 782 KN and 781 KN, respectively.
IFigs. 31-37 present the hysteresis curves for each of the used records.

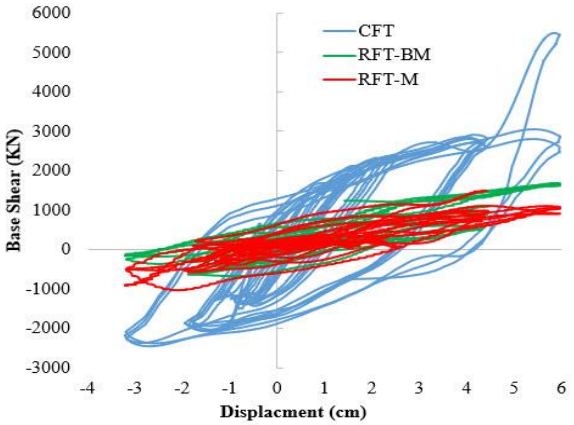

Fig. 31: Hysteresis curve under the KOBE Amagasaki Earthquake

The area under the curve of hysteresis for the CFT, RFT-BM, and RFT-M frames was measured at 1340440648 (kn-mm), 131857855 (kn-mm), and 188117124 (kn-mm), respectively. This shows that the dampers on the RFT-BM and RFT-M frames could dissipate 90.2% and 86.0% of the induced energy, respectively.

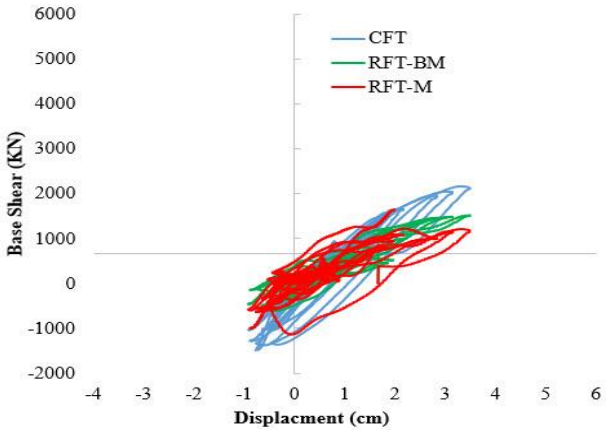

Fig. 32: Hysteresis curve under Imperial Valley El Centro Earthquake

The area under the curve of hysteresis for the CFT, RFT-BM, and RFT-M frames was measured at 58578723 (kn-mm), 36460733 (kn-mm), and 53240402 (kn-mm), respectively. This shows that the dampers on the RFT-BM and RFT-M frames could dissipate 37.8% and 9.1% of the induced energy, respectively.

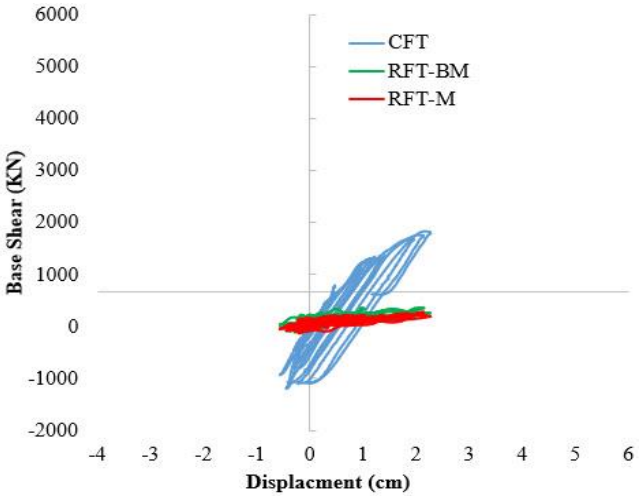

Fig. 33: Hysteresis curve under Tabas Earthquake

The area under the curve of hysteresis for the CFT, RFT-BM, and RFT-M frames was measured at 47795421 (kn-mm), 15218616 (kn-mm), and 11296898 (kn-mm), respectively. This shows that the dampers on the RFT-BM and RFT-M frames could dissipate 68.2% and 76.4% of the induced energy, respectively.

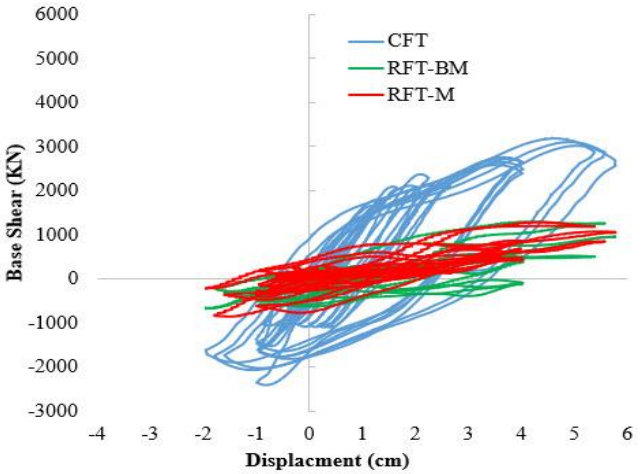

Fig. 34: Hysteresis curves under the Northridge Earthquake

The area under the curve of hysteresis for the CFT, RFT-BM, and RFT-M frames was measured at 87161738 (kn-mm), 10426431 (kn-mm), and 11692592 (kn-mm), respectively. This shows that the dampers on the RFT-BM and RFT-M frames could dissipate 83% and 86.5% of the induced energy, respectively.

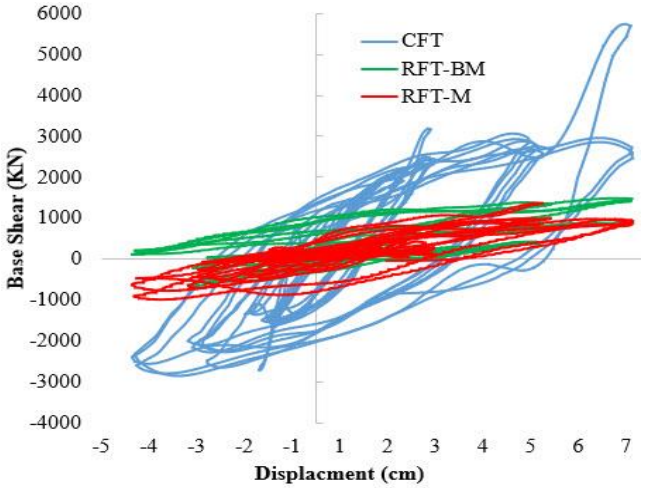

Fig. 35: Hysteresis curves under the San Fernando Earthquake

The area under the curve of hysteresis for the CFT, RFT-BM, and RFT-M frames was measured at 1673689788 (kn-mm), 159284446 (kn-mm), and 265945367 (kn-mm), respectively. This shows that the dampers on the RFT-BM and RFT-M frames could dissipate 90.5% and 84.1% of the induced energy, respectively.

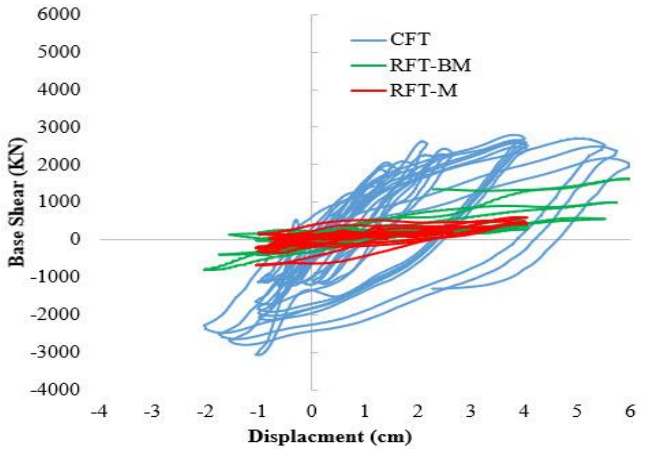

Fig. 36: Hysteresis curves under the Duzce Bolu Earthquake

The area under the curve of hysteresis for the CFT, RFT-BM, and RFT-M frames was measured at 58034863 (kn-mm), 24137805 (kn-mm), and 19426366 (kn-mm), respectively. This shows that the dampers on the RFT-BM and RFT-M frames could dissipate 58.4% and 66.5% of the induced energy, respectively.

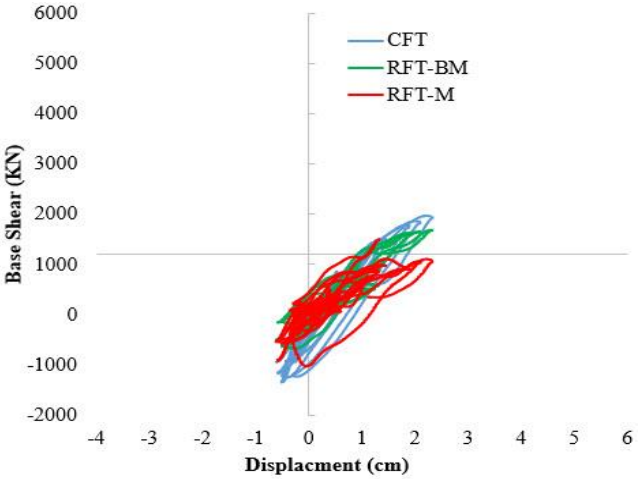

Fig. 37: Hysteresis curves under Kobe-Kakogawa Earthquake

The area under the curve of hysteresis for the CFT, RFT-BM, and RFT-M frames was measured at 58034863 (kn-mm), 58578723 (kn-mm), and 53240402 (kn-mm), respectively. This shows that the dampers on the RFT-BM and RFT-M frames could dissipate -0.9% and 8.3% of the induced energy, respectively.

In the above hysteresis curves, the base shear value in the CFT frame is higher than that of the CFT-BM and CFT-M frames due to the presence of the rotational friction damper. The rotational friction dampers have effectively dissipated the input energy, and most of the energy is dissipated mechanically.

9. Conclusion

The present article evaluated the effect of rotational friction dampers on displacement and base shear in composite steel moment-resisting frames under cyclic loading at the beam level. - Additionally, the impact of earthquake acceleration on the structure base was assessed both with and without bracing and rotational friction dampers. The following results were obtained after performing the modeling and analyses in the finite element software:

1-The base shear of the CFT-BM frame under cyclic loading decreased due to the presence of bracing and rotational friction dampers. The decreased value varied from 15 to 82%. When the base shear in the base structure is maximum, the percentage of the base shear reduction in the CFT-BM structure is maximum. Also, when the base shear in the base structure is minimum, thpercentage of the base shear reduction in the CFT-BM structure is minimum.

2-Considering the base shear curves, the CFT-M frame exhibits a performance similar to that of the CFT-BM frame under cyclic loading, indicating a 1-10% higher than that of the CFT-BM frame. Removing the two diagonal members of the bracing caused a 1-10% increase in the base shear of the CFT-M compared to the CFT-BM structure.

3-The lateral displacement of the CFT-M frame under the effect of earthquake acceleration, applied to the base of the column, decreased by 23-83% during the first 25 seconds for the CFT frame in 5 cases, increased by 15-81% in 2 cases, decreased in one case and increased in 10 cases from the 25th second to the end of the analysis.
4-The base shear of the CFT-M frame under the applied earthquake acceleration to the base of the column did not considerably change compared to the CFT frame in 3 cases, but it increased the base shear by 12-63% in 4 cases.
5-According to the studies performed by Kim et al. [12], Bonchev et al.[17], Montuori et al. [18], Shirkhani et al. [22], and Saeed-monir et al. [39], rotational friction dampers cause a reduction in the structure displacement by 30-40%, which is in agreement with the results of the present study.
6-According to the research conducted by Zhang et al. [29], friction dampers could increase the lateral stiffness of frames. Also, based on the analysis performed by Barzegar et al. [21], dampers with maximum capacity did not lead to an optimal performance. Tafakori et al. [34] concluded that friction dampers could affect structural performance in some conditions, which agrees with the results of the present study.
7-The hysteresis curves shown in Figs. 31-37 exhibit an increase in the base shear value. Rotational friction dampers have dissipated most of the seismic energy mechanically.
8-Although the reduced weight of the structure is not significant due to the removal of two diagonal members of the bracing -, the space created in the frame plane is precious for architectural purposes.

Acknowledgment

The authors thank the anonymous reviewers and editors for their careful and constructive comments.

References

[1] Ambraseys, N. and Douglas, J. (2003). Near-field horizontal and vertical earthquake ground motions, *Soil dynamics and earthquake engineering*. 23(1). 1-18.

[2] Kalkan, E. and Kunnath, S.K. (2006). Effects of fling step and forward directivity on seismic response of buildings, *Earthquake spectra*. 22(2). 367-390.

[3] Lu, C. (2012). Research on near-fault problems in earthquake engineering, *TELKOMNIKA Indonesian Journal of Electrical Engineering*. 10(5). 1033-1039.

[4] Somerville, P.G. (2005). "Engineering characterization of near fault ground motions", *Proc., NZSEE 2005 Conf.*

[5] Kohrangi, M., Vamvatsikos, D. and Bazzurro, P. (2019). Pulse-like versus non-pulse-like ground motion records: spectral shape comparisons and record selection strategies, *Earthquake Engineering & Structural Dynamics*. 48(1). 46-64.

[6] Khansefid, A. (2020). Pulse-like ground motions: Statistical characteristics, and GMPE development for the Iranian Plateau, *Soil Dynamics and Earthquake Engineering*. 134. 106164.

[7] Xu, G. and Ou, J. (2022). Seismic performance of combined rotational friction and flexural yielding metallic dampers, *Journal of Building Engineering*. 49. 104059.

[8] Veismoradi, S., Yousef-beik, S.M.M., Zarnani, P. and Quenneville, P. (2021). Development and parametric study of a new self-centering rotational friction damper, *Engineering Structures*. 235. 112097.

[9] Javidan, M.M. and Kim, J. (2019). Seismic retrofit of soft-first-story structures using rotational friction dampers, *journal of structural engineering*. 145(12). 04019162.

[10] Mirzabagheri, S., Sanati, M., Aghakouchak, A. and Khadem, S. (2015). Experimental and numerical investigation of rotational friction dampers with multi units in steel frames subjected to lateral excitation, *Archives of civil and mechanical engineering*. 15(2). 479-491.

[11] Eldin, M.N., Kim, J. and Kim, J. (June 2018). Optimum distribution of steel slit-friction hybrid dampers based on life cycle cost, *Steel and Composite Structures*. 27(5). 633-646.

[12] Kim, H.-J. and Christopoulos, C. (2008). Friction damped posttensioned self-centering steel moment-resisting frames, *Journal of Structural Engineering*. 134(11). 1768-1779.

[13] Kim, J., Kim, M. and Eldin, M.N. (November 2017). Optimal distribution of steel plate slit dampers for seismic retrofit of structures, *Steel and Composite Structures*. 25(4). 473-484.

[14] Kim, J. and An, S. (2017). Optimal distribution of friction dampers for seismic retrofit of a reinforced concrete moment frame, *Advances in Structural Engineering*. 20(10). 1523-1539.

[15] Anoushehei, M., Daneshjoo, F., Mahboubi, S. and Hashemi, M. (November and December 2018). Empirical evaluation of cyclic behavior of rotational friction dampers with different metal pads, *Scientia Iranica*. 25(6). 3021-3029.

[16] Duan, X., Zeng, Z., Liu, X., Luo, Y. and Ma, Y. (2024). Experimental and numerical study of locking steel plate damper for seismic resistance, *Journal of Constructional Steel Research*. 218. 108719.

[17] Jarrahi, H., Asadi, A., Khatibinia, M., Etedali, S. and Samadi, A. (September 2020). Simultaneous optimization of placement and parameters of rotational friction dampers for seismic-excited steel moment-resisting frames, *Soil Dynamics and Earthquake Engineering*. 136. 106193.

[18] Morgen, B.G. and Kurama, Y.C. (2008). Seismic response evaluation of posttensioned precast concrete frames with friction dampers, *Journal of Structural Engineering*. 134(1). 132-145.

[19] Moradi, R. and Kalilzadeh, V.E. (2021). General Study of New Ideas and Practical of Friction Dampers for Passive Vibration Control of Structures, *Quarterly Research Journal of Technical and Vocational University*. 17. 231-248. (in persian).

[20] Bonchev, G., Belev, B. and Mualla, I. (2017). 11.32: Linked columns with friction dampers as a technique for seismic retrofit of steel moment resisting frames, *ce/papers*. 1(2-3). 3092-3099.

[21] Montuori, R., Nastri, E. and Piluso, V. (2014). Theory of plastic mechanism control for the seismic design of braced frames equipped with friction dampers, *Mechanics Research Communications*. 58. 112-123.

[22] Naeem, A. and Kim, J. (July 2020). Seismic retrofit of structures using rotational friction dampers with restoring force, *Advances in Structural Engineering*. 23(16). 1369433220939213.

[23] Liu, Y., Chen, X. and Tagawa, H. (2024). Beam-to-column connection with double-stage yield buckling-restrained steel bar dampers, *Journal of Constructional Steel Research*. 212. 108278.

[24] Qu, Z., Ji, X., Shi, X., Wang, Y. and Liu, H. (January 2020). Cyclic loading test of steel coupling beams with mid-span friction dampers and RC slabs, *Engineering Structures*. 203. 109876.

[25] Vatandoost, H., Abdalaziz, M., Sedaghati, R. and Rakheja, S. (2024). Development of a Prandtl-Ishlinskii hysteresis model for a large capacity magnetorheological fluid damper, *Journal of Vibration and Control*. 31(1-2). 151.

[26] Barzegar, V., Laflamme, S., Downey, A., Li, M. and Hu, C. (October 2020). Numerical evaluation of a novel passive variable friction damper for vibration mitigation, *Engineering Structures*. 220. 110920.

[27] Shirkhani, A., Mualla, I.H., Shabakhty, N. and Mousavi, S.R. (2015). Behavior of steel frames with rotational friction dampers by endurance time method, *Journal of Constructional Steel Research*. 107. 211-222.

[28] Shariatmadar, H. and Abbaszadeh, H. (2009). Modeling of Buckling Restrained Braces Subjected to Dynamic loads, *journal of Modeling in engineering*. 4(18). 1-11 (in persian).

[29] Yildirim, S., Kalyoncuoglu, A., Erkus, B. and Tonguc, Y. (2015), *Seismic Retrofit of Industrial Precast Concrete Structures Using Friction Dampers: Case Study from Turkey*

[30] Langley, M., Sellers, V. and Marshall, J. (October 2020). Experimental and Analytical Testing of a Rotational Friction Connection for Metal Buildings with Hard Walls, *Journal of Structural Engineering*. 146(10). 04020212.

[31] Zahrai, S.M., Moradi, A. and Moradi, M. (2015). Using friction dampers in retrofitting a steel structure with masonry infill panels, *Steel and Composite Structures*. 19(2). 309-325.

[32] Hosseini, M., Fekri, M. and Yekrangnia, M. (2016). Seismic performance of an innovative structural system having seesaw motion and columns equipped with friction dampers at base level, *The Structural Design of Tall and Special Buildings*. 25(16). 842-865.

[33] Guo, W., Zeng, C., Gou, H., Hu, Y., Xu, H. and Guo, L. (2019). Rotational friction damper's performance for controlling seismic response of high speed railway bridge-track system, *Computer Modeling in Engineering & Sciences*. 120(3). 491-515.

[34] Zhang, A., Zhang, Y., Liu, A., Shao, D. and Li, Q. (2019). Performance study of self-centering steel frame with intermediate columns containing friction dampers, *Engineering Structures*. 186. 382-398.

[35] Oance, I. and Gelmambet, S. (2020), *Seismic Analysis of Steel Structures Using Friction Dampers*, IOP Publishing

[36] Santos, A.F., Santiago, A., Latour, M. and Rizzano, G. (2019). Analytical assessment of the friction dampers behaviour under different loading rates, *Journal of Constructional Steel Research*. 158. 443-459.

[37] Beheshti-Aval, S., Mahbanouei, H. and Zareian, F. (2013). A hybrid friction-yielding damper to equip concentrically braced steel frames, *International Journal of Steel Structures*. 13(4). 577-587.

[38] Zhang, Y., Liu, A., Zhang, A. and Liu, X. (2017). Seismic performance analysis of a resilient prestressed steel frame with intermediate column containing friction dampers, *Advanced Steel Construction*. 13(3). 241-257.

[39] Tafakori, E., Banazadeh, M., Jalali, S.A. and Tehranizadeh, M. (2013). Risk-based optimal retrofit of a tall steel building by using friction dampers, *The Structural Design of Tall and Special Buildings*. 22(9). 700-717.

[40] Taiyari, F., Mazzolani, F.M. and Bagheri, S. (2019). Damage-based optimal design of friction dampers in multistory chevron braced steel frames, *Soil Dynamics and Earthquake Engineering*. 119. 11-20.

[41] Lee, J. and Kim, J. (2015). Seismic performance evaluation of moment frames with slit-friction hybrid dampers, *Earthq. Struct*. 9(6). 1291-1311.

[42] Sanghai, S. and Pawade, P. (2021). Optimal placement of friction dampers in building considering nonlinearity of soil, *Innovative Infrastructure Solutions*. 6(1). 1-18.

[43] Miguel, L.F.F., Miguel, L.F.F. and Lopez, R.H. (2018). Methodology for the simultaneous optimization of location and parameters of friction dampers in the frequency domain, *Engineering Optimization*. 50(12). 2108-2122.

[44] Monir, H.S. and Zeynali, K. (2013). A modified friction damper for diagonal bracing of structures, *Journal of Constructional Steel Research*. 87. 17-30.

[45] Latour, M., D'Aniello, M., Zimbru, M., Rizzano, G., Piluso, V. and Landolfo, R. (2018). Removable friction dampers for low-damage steel beam-to-column joints, *Soil Dynamics and Earthquake Engineering*. 115. 66-81.

[46] Suk, R. and Altintaş, G. (2020). Behavior of multidirectional friction dampers, *Journal of Vibration and Control*. 26(21-22). 1969-1979.

[47] Solaimani, M. and Mahmoudi, N., M. (2020). Evaluation of resistive parameters of steel frame with Off-centre Bracing (-shape) Equipped with Rotating Friction Damper, *Journal of Structure & Steel*. 29. 33-44 (in persian).

[48] maleki, A., sattari, A. and Lotfollahi Yaghin, M.A. (2021). Improved Cyclic Behaviour of Concrete Filled Tube (CFT) Using Rotational Friction dampers and bracing, *Modares Civil Engineering journal*. 21(4). 185-203.

[49] Mualla, I., Nielsen, L., Sugisawa, M. and Suzuki, Y. (September 2012). "Large capacity dampers for buildings and structures", *15h World Conference on Earthquake Engineering, Lisbon, Portugal,2012*.

[50] Shrestha, B., Hao, H., Ibrahim, N.H. and Bi, K. (May 2016). On the effectiveness of rotational friction hinge damper

to control responses of multi-span simply supported bridge to non-uniform ground motions, *Advances in Structural Engineering*. 19(10). 1575-1591.

[51] Chen, W. and Hao, H. (April 2013). Numerical study of blast-resistant sandwich panels with rotational friction dampers, *International journal of Structural Stability and Dynamics*. 13(06). 1350014.

[52] Kim, J., Choi, H. and Min, K.W. (2011). Use of rotational friction dampers to enhance seismic and progressive collapse resisting capacity of structures, *The structural design of tall and special buildings*. 20(4). 515-537.

[53] Organization, I.R.o.I.C.P.a.B. (2018). Instructions for using dampers in design And strengthening of buildings, *Nezamfanni*. 766.

[54] ASCE (2017). 7-16 Minimum Design Loads and Associated Criteria for Buildings and Other Structures.

[55] Engineers, A. (2013). "Minimum design loads for buildings and other structures, standard asce/sei 7-10", *Reston, VA: American Society of Civil Engineers*.